IRANIAN JOURNAL OF CATALYSIS

Synthesis, characterization and photocatalytic activity of CeO$_2$-SBA-15

Hamid Reza Pouretedal[a*], Sara Basati[b]

[a]*Faculty of Applied Chemistry, Malek-ashtar University of Technology, Shahin-Shahr, Iran*
[b]*Department of Chemistry, Shahreza Branch, Islamic Azad University, Shahreza, 86145-311, Iran*

ABSTRACT

Mesoporous photocatalysts of CeO$_2$/SBA-15 are prepared by two methods of direct synthesis as solvent-usage and solvent-free methods. In solvent-usage method, CeO$_2$/SBA-15 is synthesized in acidic media. While, in solvent-free method, CeO$_2$/SBA-15, has been prepared through the novel path of directly grind cerium salt into the as-prepared samples of SBA-15 occluded with template. This method enables a large amount of cerium to be highly dispersed in the channels of mesoporous silica, also saves time and energy. The resulting composites exhibit photocatalytic activity, and the dispersed CeO$_2$ in SBA-15 illustrates a photodegradation of Congo red (CR) in aqueous solution. X-ray powder diffraction, N$_2$ adsorption-desorption and FT-IR spectroscopy are used to characterize the prepared materials.

Keywords: CeO$_2$, SBA-15, Photocatalyst, Congo red (CR), Nanoparticles.

1. Introduction

Silica-based and metal-incorporated mesoporous materials such as M41S show high surface area, uniform pore size distribution, large pore size and highly valuable potential application and thus used in the fields of catalysis, separation and adsorption [1–3]. After the discovery of MCM materials by Mobil researchers in 1992 [4], a lot of research has been done to synthesize all kinds of mesoporous siliceous materials. The efforts made on the synthesis of these mesoporous siliceous materials resulted in a wide range of materials with different pore structures, pore diameters, stabilities and adsorption capacities [3,4]. In the family of mesoporous molecular sieves, SBA-15, synthesized by Zhao et al. [5], is one of the most intensively studied mesoporous silica and synthesized with triblock copolymer as a surfactant under strong acidic condition exhibits larger pore sizes and thicker pore walls compared with M41S and should allow a higher flow rate of reactants and products in and out of the pores [5]. SBA-15, a mesoporous molecular sieve has large tailor able uniform pores (3–15 nm), exceptionally wide (50–300 Å diameter) ordered channels [6], thick amorphous silica walls (3–6 nm) and high surface areas (700–800 m^2/g). The improved hydrothermal and thermal stability, offers additional advantages as a catalyst and catalyst support. It can accommodate larger molecules than other molecular sieves. It is well known that, the pure-silica mesoporous molecular

sieves show low catalytic activity due to absence of heteroatom active sites. It can provide a new environment for host–guest chemistry to model nanocomposites of size-confined quantum dot or nanowires. Ordered, mesoporous SBA-15functionalized with organic and inorganic moieties exhibits efficient catalytic activity in a variety of organic transformations. Therefore, it is of great importance to introduce heteroatoms into the framework of mesoporous silica molecular sieves [4-6].

As usual, the hexagonal mesoporous SBA-15 synthesis in the gel of pH< 2, and high quality SBA-15 only can be obtained at pH < 1 [6]. But, it is very difficult to introduce directly other metal ions into the framework of SBA-15 due to the metal–O–Si bonds cannot form under so strong acidic hydrothermal conditions, even though the metal–O–Si bonds can form and they will be dissociated facilely. Heretofore, only a few papers reported the direct synthesis of metals-incorporated SBA-15 mesoporous molecular sieves, [7-9], and which mainly investigated the synthesis of Ti- or Al-incorporated SBA-15 [10, 11]. Generally, SBA-15 containing other heteroatoms was prepared mainly by the post synthesis method. Nevertheless, the post synthesis method usually would destroy the framework of SBA-15, due to complicated synthetic process, stern preparing condition and usage of solvent [12, 13]. On another hand, the metal oxide easily deposits in the channel or on the surface of SBA-15, which makes always the extra framework species form, irregularly distributes active sites and blocks the channel of SBA-15, and affects its catalytic

activity [14, 15]. So, the incorporation of heteroatoms into the framework of pure-silica SBA-15 is necessary and important for obtaining better catalytic performance and improving potential application in catalysis.

Cerium-containing materials are powerful one electron oxidants that are used as catalysts for the selective oxidation of organic reagents [16-18]. In spite of high activity of homogeneous catalytic systems, the current tendency is to replace the homogeneous catalysts by their immobilized counterparts, namely catalysts based on semiconductor ions incorporated into the network of micro- or mesoporous materials. The nanocrystaline CeO_2 is a potential candidate in a variety of applications [19] such as photodegradation of dyes. Several methods have been developed to synthesize ceria-based oxides, such as precipitation, micro emulsion, hydrothermal synthesis, etc [20, 21].

In this paper, we focus on direct synthesis of SBA-15 containing cerium oxide by two methods of solvent-usage and solvent-free. Our aim is to coat CeO_2 on the framework of SBA-15 and characterization of it. The performance of these materials towards the photocatalytic degradation of dyes such as Congo red, in aqueous solution was studied.

2. Experimental

2.1. Synthesis of pure-silica SBA-15

Pure-silica SBA-15 (Si-SBA-15) is synthesized by Zhao et al. method [22]. 2.0 g Pluronic P123 ($EO_{20}PO_{70}EO_{20}$, poly(ethylene glycol)- block-poly(propylene glycol)-block-poly(ethyleneglycol), average molecular weight = 5,800, Aldrich) is dissolved in a solution of 60 g HCl (2 M) and 15 g H_2O at room temperature. Then 4.5 g TEOS (tetraethyl orthosilicate, Aldrich Co.) is added into the solution under stirring at 40 ^{o}C. The resulting mixture is stirred at 40 ^{o}C for 24 h and then heated at 100 ^{o}C for another 24 h under static conditions. Finally, the resulting materials are filtered and washed with distilled water and air-dried. Finally, the product calcined to remove the template in a flow of air at 550 ^{o}C.

2.2. Synthesis of CeO$_2$/SBA-15 by solvent-usage method

9.4 mL TEOS and a calculated amount of cerium ammonium nitrate (40% w/w of Ce in CeO_2/SBA-15), are added to 30 mL aqueous HCl (0.2 M) solution. This solution is stirred for 3 h at 40 ^{o}C and then added to 63 mL aqueous HCl solution containing 4 g P123. After stirring for 24 h, this gel is transferred to the Teflon container and kept at 100 ^{o}C for 24 h. Then it is cooled to the room temperature then the obtained solid is filtered, washed by anhydrous ethanol, dried at 80 ^{o}C overnight, and heated finally to 550 ^{o}C at a heating rate of 2 ^{o}C/min and then maintained for 6 h [22].

2.3. Synthesis of CeO$_2$-SBA-15 by solvent-free method

The SBA-15 is synthesized as described in section of 2.1. Then a calculated amount of cerium ammonium nitrate is manually ground with the as-synthesized SBA-15 at room temperature and the resulting homogeneous powder

calcined in 550 ^{o}C at the rate of 2 ^{o}C/min for 5 h in air with a flow of 100 mL/min. The amount of cerium in CeO$_2$/SBA-15 is 40% w/w.

2.4. Sample characterization

N_2 adsorption isotherms is measured by the B.E.T. method using nitrogen as an adsorption gas at 77 K using a Belsorp Mini Π instrument. Samples are out gassed at 300°C for 4 h prior to surface area measurements. X-ray diffraction patterns (XRD) are determined by small (SAXS) and wide (WAXS) angle X-ray scattering with a Diffractometer Bruker D8ADVANCE Germany with anode of Cu (λ=1.5406 Å of Cu K_α) and filter of Ni. The FT-IR spectrum is recorded from KBr pellets (99 wt.% of KBr) on a Nicolet Impact 400D FT-IR spectrophotometer. The scanning electron microscopy (SEM) of CeO$_2$/SBA-15 is studied using a Philips XL 30 scanning electron microscope.

2.5. Photocatalytic tests

The photocatalytic activity of prepared photocatalysts is studied in photodegradation of Congo red (CR) dye. A 36 W mercury low pressure lamp uses as irradiation source in photodegradation experiments. The lamp and the tube are immersed in the photoreactor cell with a light path of 3.0 cm. The photoreactor is filled with 20 ml of 10 mg/L of CR and 0.1 g/L of CeO_2 (= 0.002 g) and CeO$_2$/SBA-15 (= 0.005 g) nanoparticles. The adsorption-desorption equilibrium is established at time 30 min in dark conditions. Nanoparticles of CeO_2 are prepared according to reported procedure of Pouretedal et. al. [23]. All reactants in the reactions stir using a magnetic stirrer to ensure that the suspension of the catalyst is uniform during the course of the reaction. The degradation efficiency of CR is determined with measurement of absorbance of samples by a UV-Vis spectrophotometer Carry-100 using a paired 1.0 cm quartz cell. The samples are centrifuged to remove the heterogeneous photocalatlysts before absorbance measurement. The absorbance of samples before (A_o) and after a distinct time (A_t) of irradiation and Beers' law to determination of C_o and C_t use for calculate of degradation efficiency as %D = 100 × [1- (C_t/C_o)].

3. Results and Discussion

3.1. Characterization of CeO$_2$/SBA-15

The powder XRD pattern of the SBA-15 sample is shown in Fig. 1. A well resolved XRD pattern with a prominent peak (100) and two weak peaks (110) and (200) observe at around 2θ = 1.09^o, 1.73^o and 1.97^o, respectively, which corresponding to a hexagonal lattice with unit cell parameter a_o = 93.5 Å (2θ = 1.09^o), characteristic of SBA-15 structure [24]. The XRD patterns of Ce-SBA-15 is prepared by two methods of solvent- free and solvent- usage are indicated in Figs. 1a and 1b, respectively. In solvent-free method, thanks to the rich surface silanol groups along with the unique dual pore structure of SBA-15, cerium oxides can be spontaneously is dispersed on SBA-15 during the whole
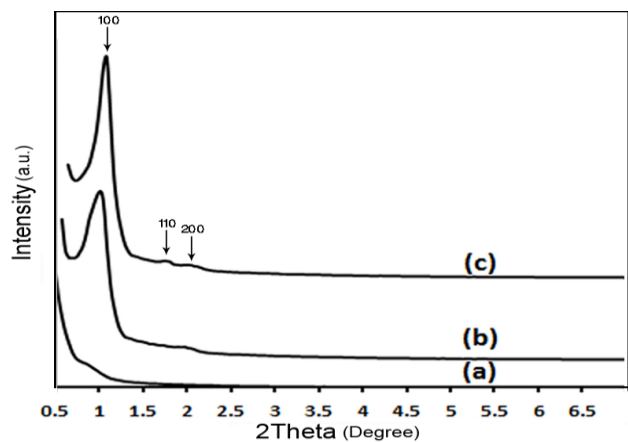
Fig. 1. The low-angle XRD patterns of Ce-SBA-15 by (a) solvent-free (b) solvent-usage method (c) pure-silica SBA-15.
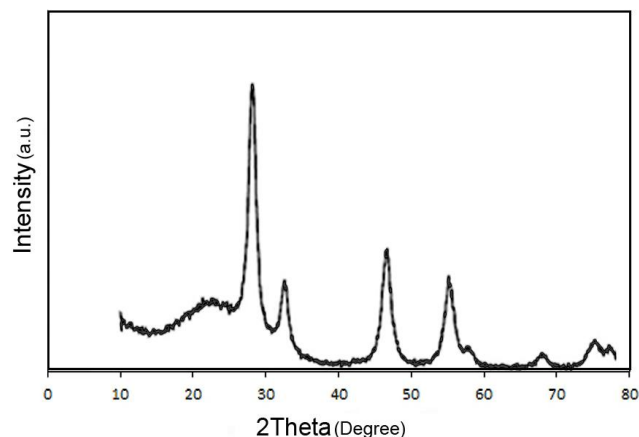
Fig. 2. The wide-angle XRD pattern of CeO_2/SBA-15 prepared by solvent-free method.

mixing–heating process, where some strong interactions occurred between the oxide species and the support. The intensity of characteristic peaks of SBA-15 is decreased obviously, owing to the pore-filling effect of CeO_2 particles that reduces the scattering contrast between the pores and the frame work of SBA-15 [25]. While, the Ce-SBA-15 is prepared by solvent- usage show XRD peaks with high intensity that is due to the low amounts of CeO_2 in substrate of SBA-15. Apparently, the cerium ions are removed by solvent in solvent-usage method.

The wide-angle XRD pattern (Fig. 2) of Ce/SBA-15

prepared by solvent- free show that there are the type diffraction peaks of CeO_2 in the XRD spectrum, which indicates that cerium dioxide disperses highly on the surface of channel wall when introducing cerium species into SBA-15 [22]. Since the size of the CeO_2 nanocrystallites at high loadings (40%) is larger than the pore size of SBA-15, it can be concluded that in the case of the highest CeO_2 loading, CeO_2 crystals have formed on the external surface. There is only a broad peak centered at about 23° to indicate the amorphous wall structure of SBA-15 [22, 26]. The peaks at $2\theta = 27.9^o, 32.8^o, 47.3^o, 55.6^o$ corresponding to CeO_2 [27]. The nanoparticles size of CeO_2 on the mesoprouse substrate are calculated 7.8 nm from the peak at $2\theta = 27.9^o$ using Scherrer's equation [28].

The N_2 adsorption–desorption isotherms of CeO_2/SBA-15 synthesized by solvent-free method are shown in Fig. 3 and the obtained data are collected in Table 1. The type IV isotherm curves well-defined step clearly indicates that these materials possess mesoporous structure [6]. The isotherms of nitrogen adsorption is exhibited an abrupt increase at $P/P_0 \sim 0.68$, which is characteristic for capillary condensation within the uniform mesopores of the materials (Fig. 3 A).

Values of specific surface area, pore volume and pore diameter, considerably decrease after introduction of 40% cerium content (Table 1). The decrease of pore volume has been observed for SBA-15 materials filled with Ce, explained by filling of micropores in the wall with the deposit. The shift in the reflections or the changing of pore diameter of Ce-SBA-15 from SBA-15, can be explained by the distinction of atomic radius of Ce^{4+} (1.02–1.06 Å) and Si^{4+}(0.39 Å) [27]. Noteworthy, the Ce–O bond length is longer than that of Si–O as well. These phenomena can relate to incorporation of cerium ions into silicate framework and the formation of CeO_2 high-dispersity species on the surface of SBA-15 [27].

The FT-IR absorption spectra of pure silica SBA-15 and Ce-incorporated SBA-15 synthesized by solvent-free method are shown in Fig. 4. The sample show a characteristic absorption band at 3432 cm^{-1} that is assigned to the vibration absorption of silanol groups (Si–O–H) situated inside the channels of SBA-15 [22]. In the range of 400–1600 cm^{-1}, three peaks at ~465, ~800, and ~1090 cm^{-1} are corresponding to the rocking, bending (or symmetric stretching), and asymmetric stretching of the

Table 1. The N_2 adsorption–desorption of Si- SBA-15and CeO_2/SBA-15 photocatalysts.

Mesoporous material	BET data			BJH data		
	S (m²/g)	P (cm³/g)	D (nm)	S (m²/g)	P (cm³/g)	D (nm)
Si-SBA-15	781.5	1.3655	6.9891	697.65	1.2984	4.03
CeO_2/SBA-15 (Solvent-free)	287.9	0.3651	4.1226	271.76	0.3021	1.35

S: Specific surface area, P: Pore volume, D: Average pore diameter
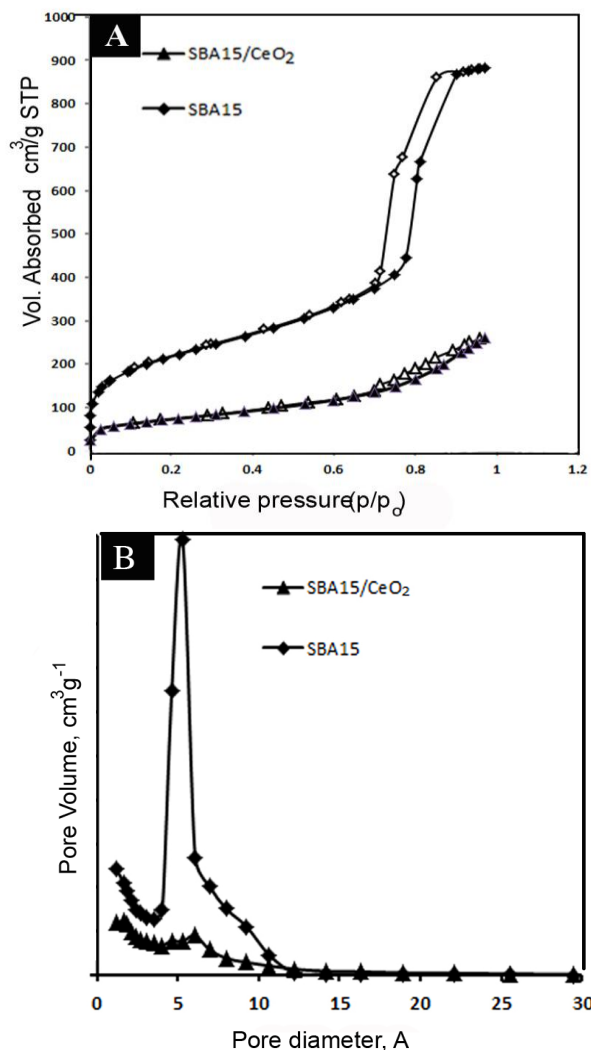
Fig. 3. Nitrogen adsorption–desorption isotherms (A) and pore size distribution (B) of SBA-15 and CeO$_2$/SBA-15 (solvent-free method).
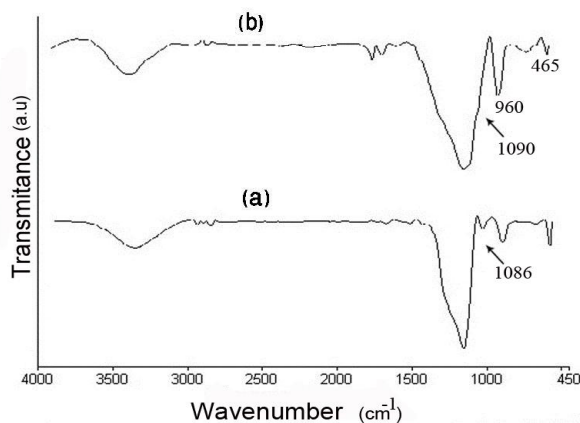
Fig. 4. IR-spectra of (a) pure-silica SBA-15 (b) Ce-SBA-15 by solvent-free method.

inter-tetrahedral oxygen atoms in SiO$_2$ of SBA-15, respectively [30]. The vibration absorption band at ~1090 cm^{-1} is assigned to υ_{as} (Si–O–Si) and its wave number decreases with increasing of the cerium in Ce-SBA-15, thus the peak at 1090 cm^{-1} of Si-SBA-15 shifts to 1087cm^{-1} of Ce-SBA-15. In general, this shift of the absorption peaks toward the lower wave number is considered an indication of Ce incorporating into the framework of silica tetrahedral. The absorption band at ~960 cm^{-1} that is observed in the pure silica SBA-15 sample, can be assigned to the stretching vibrations of Si-O in the Si–O$^-$–R$^+$ groups, as R$^+$=H$^+$ in the calcined sample, that is, υ_{as} (Si–OH) vibration presented in the framework of SBA-15 [22]. With increase of the cerium in the framework of SBA-15, the absorbance intensity of peak at 960 cm^{-1} decrease, this implies that Si–O–R or Si–OH groups are changed or consumed and transformed to the Si–O–Ce bonds [31].

The SEM image of CeO$_2$/SBA-15 synthesized by solvent-free method is shown in Fig. 5. The SEM image demonstrates that the solvent-free method can produce high 3D structure for prepared photocatalyst.

3.2. Photocatalytic activity

The photocatalytic activities of prepared photocatalysts are shown in Table 2 in photodegradation of CR. Degradation of the CR molecules is occurred under UV-Vis irradiation in the absence of any photocatalyst but at a slow rate. Irradiation in the presence of CeO$_2$ nanoparticles leads to an increase in degradation efficiency. CeO$_2$ is a semiconducting material and the onset of absorption will be at wavelengths lower than 495 nm [29]. Therefore, radiation of wavelength less than 495 nm is suitable for the transfer of electrons from the valance band to the conductance band. Therefore, electrons, e$^-$, and holes, h$^+$, are formed in the valance and conductance bands, respectively. The reaction between the positive holes and adsorbed water leads to hydroxyl species. The dye degrades by the attack of holes and hydroxyl species [30,31].

These experiments demonstrate that both UV-Vis light and photocatalyst are needed for the effective destruction of CR. The results are showed that Ce-incorporated SBA-15 samples because of their high surface areas, exhibit higher photocatalytic activity than CeO$_2$ under irradiation [32]. Also the photodegradation rate of the CeO$_2$/SBA-15 synthesized by solvent-free method is higher than the CeO$_2$/SBA-15 synthesized by solvent-usage method. This shows that the cerium species in the solvent-usage method cannot be introduced completely into the framework of SBA-15 in the solvent media.

4. Conclusion

We looked the CeO$_2$ guest has been well dispersed in mesoporous silica through the solvent-free method. Through grinding the precursors, cerium ammonium nitrate with the as prepare SBA-15 occluded with template, the guest can be penetrated inside the confined space between the template
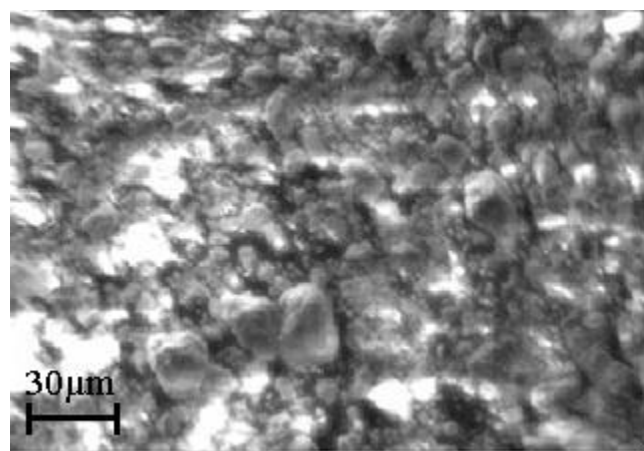
Fig. 5. SEM image of Ce-SBA-15 by solvent-free method.

aggregates and the silica walls, well dispersed in the channel of SBA-15 and converted to CeO_2 in the subsequent calcination. Apart from being energy- and time-efficient, this strategy can keep the ordered mesostructures of SBA-15 whose thermal and hydrothermal stability is higher than another mesoprouses, and enables an unexpectedly high dispersion of CeO_2, (40 wt.% Ce), to be realized in SBA-15

Table 2. The degradation efficiency of CR catalyzed by CeO_2 photocatalysts

Photocatalyst	Time (min)			
	15	30	45	60
-	10.1	13.4	25.1	31.7
CeO_2	16.1	19.4	28.2	34.4
CeO_2/SBA-15, Solvent-usage	18.0	21.1	31.4	38.2
CeO_2/SBA-15, Solvent-free	22.3	24.9	37.7	49.2

References

[1] M. Selvaraj, A. Pandurangan, P.K. Sinha, V. Krishnasamy, K.B. Lal, J. Mol. Catal. A: Chem. 186 (2002) 173-186.

[2] S.K. Jana, H. Takahashi, M. Nishida, H. Shimizu, T. Kugita, S. Namba, Appl. Catal. A: Gen. 245 (2003) 33-41.

[3] R.K. Rana, B. Viswanathan, Catal. Lett. 52 (1998) 25-29.

[4] J.S. Kresge, M.E. Leonowicz, W.J. Roth, J.C. Beck, Nature 359 (1992) 710-712.

[5] D.Y. Zhao, J.L. Feng, Q. Huo, N. Melosh, G.H. Fredrickson, B.F.Chmelka, G.D. Stucky, Science 279 (1998) 548-552.

[6] D.Y. Zhao, J.L. Feng, Q. Huo, N. Melosh, B.F.Chmelka, G.D. Stucky, J. Am. Chem. Soc. 120 (1998) 6024-6036.

[7] A. Cedeon, A. Lassoued, J.L. Bonardet, J. Fraissard, Micropor. Mesopor. Mater. 801 (2001) 44–45.

[8] W.H. Zhang, J. Lu, B. Han, M. Li, J. Xiu, P. Ying, C. Li, Chem. Mater. 14 (2002) 3413-3421.

[9] S. Wu, Y. Han, Y.C. Zou, J.W. Song, L. Zhao, Y. Di, S.Z. Liu, F.S. Xiao, Chem. Mater. 16 (2004) 486-492.

[10] A. Vinu, V. Murugesan, W. Bohlmann, M. Hartmann, J. Phys. Chem. B 108 (2004) 11496-11505.

[11] Y. Li, W.H. Zhang, L. Zhang, Q.H. Yang, Z.B. Wei, Z.C. Feng, C. Li, J. Phys. Chem. B 108 (2004) 9739-9744.

[12] M.S. Morey, S. O'Brien, S.S. Warz, G.D. Stucky, Chem. Mater. 12 (2000) 898-911.

[13] S. Sumiya, Y. Oumi, T. Uozumi, T. Sano, J. Mater. Chem. 11 (2001) 1111-1115.

[14] R. Murugavel, H.W. Roesky, Angew Chem. Int. Ed. 109 (1997) 4491-4495.

[15] Y. Han, X. Meng, H. Guan, Y. Yu, L. Zhao, X. Xu, X. Yang, S. Wu, N. Li, F. Xiao, Micropor. Mesopor. Mater. 57 (2003) 191-198.

[16] S. Mcintosh, J.M. Vohs, R.J. Gorte, Electrochim. Acta 47 (2002) 3815-3821.

[17] S. Park, R. Cracium, J.M. Vohs, R.J. Gorte, J. Electrochem. Soc. 146 (1999) 3603-3605.

[18] C. Lu, W.L. Worrell, R.J. Gorte, J.M. Vohs, J. Electrochem. Soc. 150 (2003) 354-358.

[19] S.J. Pearton, D.P. Norton, K. Ip, Y.W. Heo, T. Steiner, Prog. Mater. Sci. 580 (2005) 293-340.

[20] J.G. Li, T. Ikegami, T. Mori, T. Wada, Chem. Mater. 13 (2001) 2913-2920.

[21] P. Duran, F. Capel, D. Gutierrez, J. Tartaj, C. Moure, J. Eur. Ceram. Soc. 22 (2002) 1711-1721.

[22] Q. Dai, X. Wang, G. Chen, Yi. Zheng, G. Lu, Micropor. Mesopor. Mat. 100 (2007) 268–275.

[23] H. R. Pouretedal, A. Kadkhodaie, Chinese J. Catal. 31 (2010) 1328–1334.

[24] G.D. Mihai, V. Meynen, M. Mertens, N. Bilba, P. Cool, E.F. Vansant, J. Mater. Sci. 45 (2010) 5786–5794.

[25] W.H. Zhang, J.L. Shi, L.Z. Wang, D.S. Yan, Chem. Mater. 12 (2000) 1408-1413.

[26] F.N. Gu, M. B. Yue, Zh. Y. Wu, L. B. Sun, Y. Wang, J. H. Zhu, Luminescence. 128 (2008) 1148–1154.

[27] M.N. Timofeeva, S.H. Jhung, Y.K. Hwang, D.K. Kim, V.N. Panchenko, M.S. Melgunov, Yu. A. Chesalov, J.S. Chang, Appl. Catal. A 317 (2007) 1–10.

[28] H.P. Klug, L.E. Alexander, X-Ray Diffraction Methods for Polycrystalline and Amorphous Materials, John Wiley and Sons, New York, 1954.

[29] M. Movahedi, A.R. Mahjoub, S. Janitabar-Darzi, J. Iran. Chem. Soc. 6 (2009) 570-577.

[30] M.S. Morey, S. O'Brien, S.S. Warz, G.D. Stucky, Chem. Mater. 12 (2000) 898-911.

[31] M. Jang, J.K. Park, E.W. Shin, Micropor. Mesopor. Mater. 75 (2004) 159-168.

[32] K. De Witte, A.M. Busuioc, V. Meynen, M. Mertens, N. Bilba, G.V. Tendeloo, P. Cool, E.F. Vansant, Micropor. Mesopor. Mater. 110 (2008) 100–110.